J. Cent. South Univ. (2015) 22: 4337−4346
DOI: 10.1007/s11771-015-2982-z

Springer

Hydro-mechanical modeling of impermeable discontinuity in rock by extended finite element method

ZHENG An-xing(郑安兴), LUO Xian-qi(罗先启)

School of Naval Architecture, Ocean and Civil Engineering, Shanghai Jiao Tong University, Shanghai 200240, China

Abstract: The extended finite element method (XFEM) is a numerical method for modeling discontinuities within the classical finite element framework. The computation mesh in XFEM is independent of the discontinuities, such that remeshing for moving discontinuities can be overcome. The extended finite element method is presented for hydro-mechanical modeling of impermeable discontinuities in rock. The governing equation of XFEM for hydraulic fracture modeling is derived by the virtual work principle of the fracture problem considering the water pressure on crack surface. The coupling relationship between water pressure gradient on crack surface and fracture opening width is obtained by semi-analytical and semi-numerical method. This method simplifies coupling analysis iteration and improves computational precision. Finally, the efficiency of the proposed method for modeling hydraulic fracture problems is verified by two examples and the advantages of the XFEM for hydraulic fracturing analysis are displayed.

Key words: extended finite element method; crack; hydraulic fracture; fluid flow; coupling model; impermeable discontinuities

1 Introduction

Hydraulic fracturing is the propagation of fractures in the rock formation through the fluid pressure on crack surfaces. It is a commonly used technique in petroleum engineering to enhance reservoirs permeability and wells efficiency. Modeling of fluid-driven fracture propagation is a significant challenging problem in rock mechanics and engineering because of the strong nonlinear coupling between the viscous flow of fluid inside the fracture and fracture propagation (a moving boundary). Plus, the coupled hydro-mechanical process has the practical importance in design and safety assessment in many engineering fields, such as geotechnical engineering and environmental engineering.

The problem of modeling fluid-driven fractures was studied by many contributors during the last decades from an analytical perspective [1−5]. These solutions usually suffer from the limitations of the analytical models. To deal with more complex fracture geometries, numerical tools were developed to simulate the hydraulic fracture problem [6]. These tools applied are finite element method (FEM), boundary element method (BEM), finite difference method (FDM), distinct element method (DEM) and so on. The finite element method has been most widely used in modelling the hydraulic fracture propagation in homogeneous rocks. For example, SIMONI and SECCHI [7] and SECCHI et al [8] modeled the hydraulic cohesive crack growth by the finite element method with mesh adaptation; SEGURA and CAROL [9] proposed a hydro-mechanical formulation for geomaterials with pre-existing discontinuities based on the finite element method with zero-thickness interface elements. However, the standard finite element model requires remeshing after crack propagation and the finite element mesh needs to conform to the crack geometry, and thus is computationally expensive.

The extended finite element method (XFEM) is a numerical method for modeling discontinuities within a standard finite element framework. It was first introduced by BELYTSCHKO and BLACK [10] at Northwest University in 1999. In the XFEM, a Heaviside function and the two-dimensional asymptotic crack-tip displacement fields are added to the finite element approximation to account for discontinuity of the crack surface and stress singularity near the crack tip respectively. This enables the domain to be modeled by finite elements without explicitly meshing the crack surfaces, and hence crack growth simulations can be carried out without remeshing [10]. The extended finite element method (XFEM) is an effective method for discontinuous problems in mechanics within a standard finite element framework and maintains all advantages of

Foundation item: Project(2011CB013505) supported by the National Basic Research Program of China; Project(51279100) supported by the National Natural Science Foundation of China
Received date: 2014−10−10; **Accepted date:** 2015−01−30
Corresponding author: LUO Xian-qi, Professor, PhD; Tel: +86−21−34207903; E-mail: luoxianqi@sjtu.edu.cn

the common finite element method on the basis of the partition of unity, so this method facilitates the modeling of the propagating crack. Due to the unique advantage of XFEM for fracture analysis, it has been employed to investigate the hydraulic fracture problems. The method was employed by REN et al [11] in modeling of hydraulic fracturing in concrete by imposing a constant pressure value along the crack faces. The technique was also employed by LECAMIPON [12] in hydraulic fracture problems using the special crack-tip functions in the presence of internal pressure inside the crack. The XFEM was recently employed by MOHAMADNEJAD and KHOEI [13] in hydro-mechanical modeling of deformable, progressively fracturing porous media interacting with the flow of two immiscible, compressible wetting and non-wetting pore fluids. The main objective of this work is to develop a coupled numerical model on the basis of the extended finite element method in conjunction with a hydro-mechanical model for the modeling of the hydraulic fracture propagation in rock. Finally, two numerical examples are presented to demonstrate the capability and the efficiency of the developed model in the simulation of the hydraulic fracture propagation in rock. The effect of some parameters that have an influence on the hydraulic fracture propagation is studied further.

2 Hydraulic fracture model with XFEM

2.1 XFEM approximation for cracks

In XFEM, special enriched shape functions are added to enrich the finite element displacement using the framework of partition of unity to model the discontinuities of cracks. The displacement approximation for an isotropic linear elastic material with a crack takes the following form:

$$\boldsymbol{u}=\sum_{i\in\Omega} N_i(x)\left[\boldsymbol{u}_i+\underbrace{H(x)\boldsymbol{a}_i}_{i\in\Omega_\Gamma}+\underbrace{\sum_{l=1}^{4}F_l(x)\boldsymbol{b}_i^l}_{i\in\Omega_\Lambda}\right] \tag{1}$$

where Ω is the entire domain; $N_i(x)$ is the traditional finite element shape function; $\boldsymbol{u}_i$ is the traditional degree of freedom; Ω_Γ is the domain cut by the crack; $H(x)$ is the Heaviside enrichment; $\boldsymbol{a}_i$ denotes the nodal enriched degree of freedom associated with the discontinuous Heaviside function; Ω_Λ is the domain containing the crack tip; $F_l(x)$ is the crack tip enrichment; $\boldsymbol{b}_i^l$ is the nodal degree of freedom corresponding to the near-tip function.

For an element completely cut by a crack, the Heaviside enrichment function is given as [14]

$$H(x)=\begin{cases}+1, & (\boldsymbol{x}-\boldsymbol{x}^*)\cdot\boldsymbol{n}>0\\ -1, & \text{otherwise}\end{cases} \tag{2}$$

where $\boldsymbol{x}$ is a sample (Gauss) point; $\boldsymbol{x}^*$ (lies on the crack) is the closest point to $\boldsymbol{x}$; $\boldsymbol{n}$ is the unit outward normal to the crack at $\boldsymbol{x}^*$.

For the isotropic elasticity, the near tip displacement field takes the form of the following four functions [15]:

$$F_l(x)=\sqrt{r}\left[\sin\left(\frac{\theta}{2}\right)\ \cos\left(\frac{\theta}{2}\right)\ \sin\theta\cos\left(\frac{\theta}{2}\right)\ \sin\theta\sin\left(\frac{\theta}{2}\right)\right] \tag{3}$$

where (r, θ) are the polar coordinates in the local crack-tip coordinate system (see Fig. 1). A node should be enriched by both Eqs. (2) and (3), and only Eq. (3) is used as shown in Fig. 2, in which the nodes with circle are enriched by the Heaviside step function, and the nodes with square are enriched by the crack tip enrichment functions.

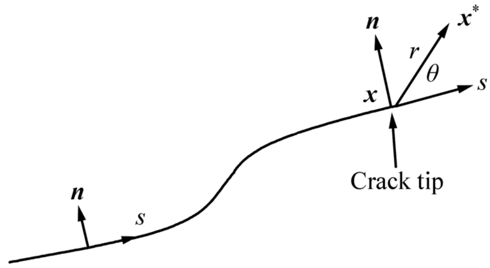

Fig. 1 Local coordinate system

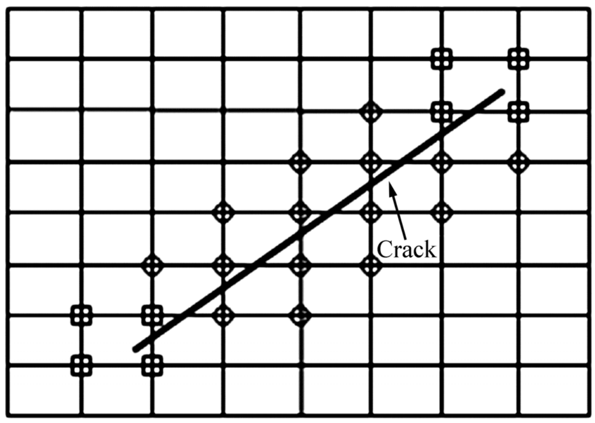

Fig. 2 Nodes enriched with enrichment functions

According to Eq. (1), the displacement discontinuity between the two surfaces of the crack can be obtained as

$$\boldsymbol{w}=\boldsymbol{u}^+-\boldsymbol{u}^-=2\sum_{i\in\Omega_\Gamma}N_i\boldsymbol{a}_i+2\sqrt{r}\sum_{i\in\Omega_\Lambda}N_i\boldsymbol{b}_i^1 \tag{4}$$

where $\boldsymbol{w}$ is the separation between the two faces of the crack.

2.2 Governing equations

Consider a two-dimensional plane strain model in a homogeneous, isotropic, impermeable medium, which will be employed to model the hydraulic fracture propagating. A small elastic deformation domain Ω

contains an edge crack described by Γ_c as shown in Fig. 3. We assume quasi-static loading by a body force $\boldsymbol{b}$ and traction $\boldsymbol{t}$ imposed on the part Γ_t of the boundary. The domain is constrained by prescribed displacement $\boldsymbol{u}$ imposed on the part Γ_u of the boundary. The prescribed stress and displacement fields are $\boldsymbol{\sigma}$ and $\boldsymbol{u}$, respectively. The crack face Γ_c is distinguished into two parts Γ_c^+ and Γ_c^- in which $\Gamma_c=\Gamma_c^+\cup\Gamma_c^-$ and the normal vectors to Γ_c^+ and Γ_c^- are denoted by $\boldsymbol{n}^+$ and $\boldsymbol{n}^-$. The fracture propagation is mainly dependent on the water pressure $\boldsymbol{p}$ including $\boldsymbol{p}^+$ and $\boldsymbol{p}^-$, which are acted on the boundary Γ_c^+ and Γ_c^-, respectively.

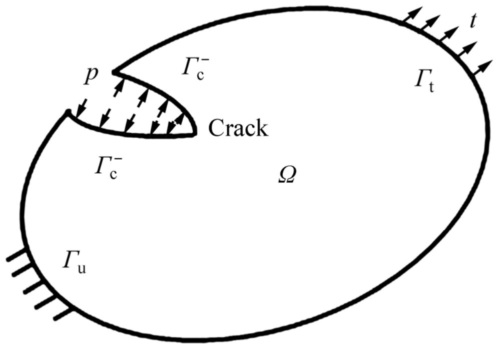

Fig. 3 Geometry of discontinues domain and its boundary conditions

In this model, the equilibrium equation and the boundary condition are as follows:

$$\begin{cases}\nabla\boldsymbol{\sigma}+\boldsymbol{b}=0, \text{on } \Omega \\ \boldsymbol{\sigma}\cdot\boldsymbol{n}=\boldsymbol{t}, \text{ on } \Gamma_t \\ \boldsymbol{\sigma}\cdot\boldsymbol{n}^-=-\boldsymbol{\sigma}\cdot\boldsymbol{n}^+=\boldsymbol{p}^+=-\boldsymbol{p}^-=\boldsymbol{p}, \text{on } \Gamma_c\end{cases} \tag{5}$$

The stress field insider the domain Ω is expressed in terms of the isotropic, linear elastic constitutive law as

$$\boldsymbol{\sigma}=\boldsymbol{D}:\boldsymbol{\varepsilon} \tag{6}$$

where $\boldsymbol{D}$ is Hooke's tensor.

The weak form of the equilibrium equations can be written as

$$\int_\Omega \boldsymbol{\sigma}:\delta\boldsymbol{\varepsilon}\mathrm{d}\Omega=\int_\Omega \boldsymbol{b}\cdot\delta\boldsymbol{u}\mathrm{d}\Omega+\int_{\Gamma_t}\boldsymbol{t}\cdot\delta\boldsymbol{u}\mathrm{d}S+\int_{\Gamma_c^+}\boldsymbol{p}^+\cdot\delta\boldsymbol{u}^+\mathrm{d}S+\int_{\Gamma_c^-}\boldsymbol{p}^-\cdot\delta\boldsymbol{u}^-\mathrm{d}S \tag{7}$$

where $\delta\boldsymbol{u}$ is an arbitrary virtual displacement and $\delta\boldsymbol{\varepsilon}$ is the corresponding virtual strain.

For the water pressure on the crack surfaces, we have $\boldsymbol{p}^+=-\boldsymbol{p}^-=\boldsymbol{p}$. So, the last two terms of the right-hand side of Eq. (7) can be expressed as

$$\int_{\Gamma_c^+}\boldsymbol{p}^+\cdot\delta\boldsymbol{u}^+\mathrm{d}S+\int_{\Gamma_c^-}\boldsymbol{p}^-\cdot\delta\boldsymbol{u}^-\mathrm{d}S=\int_{\Gamma_c}\boldsymbol{p}\cdot(\delta\boldsymbol{u}^+-\delta\boldsymbol{u}^-)\mathrm{d}S \tag{8}$$

Substituting Eq. (8) into Eq. (7), Eq. (7) can be rewritten as

$$\int_\Omega \boldsymbol{\sigma}:\delta\boldsymbol{\varepsilon}\mathrm{d}\Omega=\int_\Omega \boldsymbol{b}\cdot\delta\boldsymbol{u}\mathrm{d}\Omega+\int_{\Gamma_t}\boldsymbol{t}\cdot\delta\boldsymbol{u}\mathrm{d}S+\int_{\Gamma_c}\boldsymbol{p}\cdot(\delta\boldsymbol{u}^+-\delta\boldsymbol{u}^-)\mathrm{d}S \tag{9}$$

By defining $\delta\boldsymbol{w}=\delta\boldsymbol{u}^+-\delta\boldsymbol{u}^-$, where $\delta\boldsymbol{u}^+$ is the separation between the two surfaces of the crack, the week form of the hydraulic fracturing equilibrium equation can be given by

$$\int_\Omega \boldsymbol{\sigma}:\delta\boldsymbol{\varepsilon}\mathrm{d}\Omega=\int_\Omega \boldsymbol{b}\cdot\delta\boldsymbol{u}\mathrm{d}\Omega+\int_{\Gamma_t}\boldsymbol{t}\cdot\delta\boldsymbol{u}\mathrm{d}S+\int_{\Gamma_c}\boldsymbol{p}\cdot\delta\boldsymbol{w}\mathrm{d}S \tag{10}$$

2.3 Discretized equations

Substitution of the displacement approximations (Eq. (1)) and the constitutive equation (Eq. (6)) into Eq. (10), the following discrete system of linear equations is obtained

$$\boldsymbol{Kd}=\boldsymbol{f} \tag{11}$$

where $\boldsymbol{d}$ is the vector of degrees of nodal freedom (for both classical and enriched ones), defined as

$$\boldsymbol{d}=\{\boldsymbol{u}_i\ \boldsymbol{a}_i\ \boldsymbol{b}_i^1\ \boldsymbol{b}_i^2\ \boldsymbol{b}_i^3\ \boldsymbol{b}_i^4\}^\mathrm{T} \tag{12}$$

$\boldsymbol{K}$ and $\boldsymbol{f}$ are the global stiffness matrix and external force vector, respectively.

The global matrix is calculated by assembling the matrix of each element. For each element e, $\boldsymbol{K}$ may be calculated as

$$\boldsymbol{K}_\mathrm{e}=\int_{\Omega^\mathrm{e}}(\boldsymbol{B}_r)^\mathrm{T}\boldsymbol{DB}_s\mathrm{d}\Omega \tag{13}$$

where r, s=u, a, b; Ω^e is an element such that the crack lies along the edges of these elements; $\boldsymbol{B}_u$, $\boldsymbol{B}_a$, $\boldsymbol{B}_b$ are the matrices of shape function derivatives which are given by

$$\begin{cases}\boldsymbol{B}_u=\begin{bmatrix}N_{i,x} & 0\\ 0 & N_{i,y}\\ N_{i,y} & N_{i,x}\end{bmatrix}\\ \boldsymbol{B}_a=\begin{bmatrix}(N_iH)_{,x} & 0\\ 0 & (N_iH)_{,y}\\ (N_iH)_{,y} & (N_iH)_{,x}\end{bmatrix}\\ \boldsymbol{B}_b=[\boldsymbol{B}_{b1}\ \boldsymbol{B}_{b2}\ \boldsymbol{B}_{b3}\ \boldsymbol{B}_{b4}]\\ \boldsymbol{B}_{bl}=\begin{bmatrix}(N_iF_l)_{,x} & 0\\ 0 & (N_iF_l)_{,y}\\ (N_iF_l)_{,y} & (N_iF_l)_{,x}\end{bmatrix}\end{cases} \tag{14}$$

where l=1−4; $N_{i,x}$ and $N_{i,y}$ are the derivatives of N_i with respect to x and y, respectively; $(N_iH)_x$ and $(N_iH)_y$ is the derivatives of (N_iH) with respect to x and y, respectively; $(N_iF_l)_x$ and $(N_iF_l)_y$ is the derivatives of (N_iH) with respect to x and y, respectively.

$\boldsymbol{f}$ is the equivalent node force vector of body force $\boldsymbol{b}$, traction $\boldsymbol{t}$ and water pressure $\boldsymbol{p}$ which is given by

$$\boldsymbol{f}=\{\boldsymbol{f}_u\ \boldsymbol{f}_a\ \boldsymbol{f}_{b1}\ \boldsymbol{f}_{b2}\ \boldsymbol{f}_{b3}\ \boldsymbol{f}_{b4}\}^{\mathrm{T}} \tag{15}$$

where the vectors that appear in Eq. (15) are defined as

$$\begin{cases}\boldsymbol{f}_u=\int_{\Gamma_\mathrm{t}}\mathrm{N}_i\boldsymbol{t}\mathrm{d}\Gamma_\mathrm{t}+\int_{\Omega^\mathrm{e}}N_i\boldsymbol{b}\mathrm{d}\Omega\\ \boldsymbol{f}_a=\int_{\Gamma_\mathrm{t}}N_iH\boldsymbol{t}\mathrm{d}\Gamma_\mathrm{t}+\int_{\Omega^\mathrm{e}}N_iH\boldsymbol{b}\mathrm{d}\Omega+2\int_{\Gamma_\mathrm{c}}\boldsymbol{n}\cdot N_i\boldsymbol{p}\mathrm{d}\Gamma\\ \boldsymbol{f}_{bl}=\int_{\Gamma_\mathrm{t}}N_iF_l\boldsymbol{t}\mathrm{d}\Gamma+\int_{\Omega^\mathrm{e}}N_iF_l\boldsymbol{b}\mathrm{d}\Omega+2\int_{\Gamma_\mathrm{c}}\boldsymbol{n}\sqrt{r}\cdot N_i\boldsymbol{p}\mathrm{d}\Gamma\end{cases} \tag{16}$$

where l=1−4; N_i is finite element shape function.

It can be shown that for an element which is cut by the crack, water pressure vector components are related to the regular degrees of freedom vanish. Only the additional degrees of freedom contribute to the external nodal force of the crack interface.

2.4 Numerical integration method

To construct the integrals on the crack surface, it is necessary to discretize Γ_c. In traditional finite element discretization, nodes must be placed on the element faces which align with the crack surface. In XFEM, since the crack and mesh geometry are independent, we first divide Γ_c into one-dimensional segments. The segments are determined according to the interaction of the crack geometry with the mesh. In order to numerically integrate the terms in Eq. (16) on Γ_c, an enough number of Gauss points are used along each of the one-dimensional segments, as shown in Fig. 4.

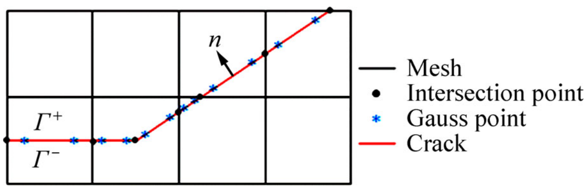

Fig. 4 Gauss points on crack segments for crack surface

3 Hydro-mechanical coupling model

3.1 Fluid-flow model of single crack

A hydro-mechanical model of rock with a single fracture initially filled by saturation water was introduced by LI et al [16]. It is assumed that the fracturing fluid is an incompressible, uniform and Newtonian viscous fluid. The flow pattern is one-dimensional laminar flow and differential equation of water pressure distribution due to hydraulic fracturing is obtained by the finite control volume approach.

The pressure gradient and the fracture width in the domain filled with fluid are related by the basic equation in the approximation of lubrication theory [7]:

$$q=-\frac{w^3}{12\mu}\frac{\partial p}{\partial x} \tag{17}$$

where q is the local flow rate; μ is the dynamic viscosity of the fracturing fluid; w is the local fracture width; p denotes the fluid pressure in the fracture.

The fracturing fluid is considered to be incompressible, so the mass conservation equation for the fluid may be expressed as

$$\frac{\partial q}{\partial x}=\frac{\partial w}{\partial t} \tag{18}$$

Equation (18) ignores any leak-off from the fracture surface into the rock formation.

Through Eq. (17), we can obtain the following differential equation:

$$\frac{\partial^2 p}{\partial x^2}+\frac{3}{w}\frac{\partial w}{\partial x}\frac{\partial p}{\partial x}=-\frac{12\mu}{w^3}\frac{\partial q}{\partial x} \tag{19}$$

Substituting of Eq. (18) into Eq. (19) leads to differential equation of water pressure distribution:

$$\frac{\partial^2 p}{\partial x^2}+\frac{3}{w}\frac{\partial w}{\partial x}\frac{\partial p}{\partial x}=-\frac{12\mu}{w^3}\frac{\partial w}{\partial t} \tag{20}$$

The solution of Eq. (20) is approximated using finite differencing techniques, and the derivative of w with respect to x or time t can be approximated as

$$\left(\frac{\partial^2 p}{\partial x^2}\right)_i^{t+1}+\frac{3}{w_i^{t+1}}\left(\frac{w_{i+1}^{t+1}-w_i^{t+1}}{\Delta x_i}\right)_i^{t+1}\left(\frac{\partial p}{\partial x}\right)_i^{t+1}=-\frac{12\mu}{(w_i^{t+1})^3}\frac{w_i^{t+1}-w_i^t}{\Delta t} \tag{21}$$

where i represents the ith control volume and Δx_i is the length of the ith control volume as shown in Fig. 5.

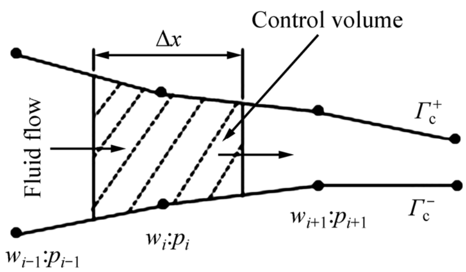

Fig. 5 Dynamic model of flow in fracture

The hydraulic fracturing in fields of water conservancy, hydropower and mining engineering is produced by natural hydraulic power. Its boundary conditions are different from those in artificial hydraulic fracturing applied in fields of petroleum and natural gas engineering. The boundary conditions for hydraulic fracturing problem of constant head and large reservoir water capacity at the edge of crack can be approximated as

$$\left(\frac{\partial p}{\partial x}\right)_{i=1}^{t+1}\Bigg|_{x=0} = 0 \tag{22}$$

Equation (21) is an order ordinary differential equation for $\partial p/\partial x$ combined with boundary condition of Eq. (22), and the following equation can be obtained as [16]

$$\left(\frac{\partial p}{\partial x}\right)_i^{t+1} = \left(e^{-\frac{3x}{w_i^{t+1}}\frac{w_{i+1}^{t+1}-w_i^{t+1}}{\Delta x_i}} - 1\right)\frac{4\mu}{(w_i^{t+1})^2}\frac{\Delta x_i}{w_{i+1}^{t+1}-w_i^{t+1}}\cdot \frac{w_i^{t+1}-w_i^t}{\Delta t} \tag{23}$$

Now, the differential Eq. (23) is obtained, which can be implicitly expressed in terms of the relative water pressure gradient in the fracture and fracture width. Starting from crack front and combined with the hydraulic boundary condition, the distribution of water pressure on the crack surfaces is given by

$$p_{i+1}^{t+1} = p_i^{t+1} + \left(\frac{\partial p}{\partial x}\right)_i^{t+1}\Delta x_i \tag{24}$$

3.2 Equivalent hydraulic aperture

The differential Eq. (23) describing the internal water pressure distribution in rock fractures formed by hydraulic fracturing is obtained under the assumption that the crack surfaces are perfectly smooth. However, the crack surfaces in rock are rough in fact. Considering the crack surface roughness effects on fluid flow in rock joints, an empirical equation proposed by BARTON [17] for the analysis of the relationship between the equivalent hydraulic aperture and the theoretical aperture is adopted herein, which is given by

$$w_{\mathrm{eq}} = JRC^{2.5}/(w/w_{\mathrm{eq}})^2 \tag{25}$$

where w_{eq} is the equivalent hydraulic aperture; w is the theoretical aperture. The units of w_{eq} and w are microns. JRC is the joint roughness coefficient and the values of JRC range from 0 to 20. The influence of roughness decreases as the fracture opens (increasing w) and w/w_{eq} approaches 1.0 [18].

4 Stress intensity factor evaluation and crack growth criterion

4.1 Stress intensity factor evaluation

An interaction integral method [19] is used for calculating the stress intensity factor (SIF) at the tip of the crack. The coordinates are taken to be the local crack tip co-ordinates with the x_1-axis parallel to the crack faces. The domain form of interaction integral is given by

$$M^{(1,2)} = \int_A\left[\sigma_{ij}^{(1)}\frac{\partial u_i^{(2)}}{\partial x_1} + \sigma_{ij}^{(2)}\frac{\partial u_i^{(1)}}{\partial x_1} - W^{(1,2)}\delta_{1j}\right]\frac{\partial Q}{\partial x_j}\mathrm{d}A - \int_{\Gamma_c}\left(p_j^{(1)}\frac{\partial u_i^{(2)}}{\partial x_1} + p_j^{(2)}\frac{\partial u_i^{(1)}}{\partial x_1}\right)Q\mathrm{d}\Gamma \tag{26}$$

where σ_{ij}, ε_{ij} and u_i represents stress component, strain component and displacement component, respectively; p_j represents water pressure on the crack surfaces; δ_{1j} is the Kronecker delta; A is an area surrounding the crack tip; Q is a weighting function; $W^{(1,2)}$ represents the strain energy density for states 1 and 2; $M^{(1,2)}$ is called the interaction integral for states 1 and 2; the states 1 and 2 depict the actual and the auxiliary states, respectively. Field variables for the actual state are obtained by the XFEM solution and those for auxiliary state are chosen as the crack tip asymptotic fields [20].

Strain energy density $W^{(1,2)}$ is given as

$$W^{(1,2)} = \frac{1}{2}(\sigma_{ij}^{(1)}\varepsilon_{ij}^{(2)} + \sigma_{ij}^{(2)}\varepsilon_{ij}^{(1)}) \tag{27}$$

Expanding and rearranging terms from Eq. (27) give

$$M^{(1,\mathrm{aux})} = \int_A\left[\left(\sigma_x\frac{\partial u_x^{\mathrm{aux}}}{\partial x} + \tau_{xy}\frac{\partial u_y^{\mathrm{aux}}}{\partial x} + \sigma_x^{\mathrm{aux}}\frac{\partial u_x}{\partial x} + \tau_{xy}^{\mathrm{aux}}\frac{\partial u_y}{\partial x} - \sigma_{ij}\varepsilon_{ij}^{\mathrm{aux}}\right)\frac{\partial Q}{\partial x} + \left(\tau_{xy}\frac{\partial u_x^{\mathrm{aux}}}{\partial x} + \sigma_y\frac{\partial u_y^{\mathrm{aux}}}{\partial x} + \tau_{xy}^{\mathrm{aux}}\frac{\partial u_x}{\partial x} + \sigma_y^{\mathrm{aux}}\frac{\partial u_y}{\partial x}\right)\frac{\partial Q}{\partial y}\right]\mathrm{d}A - \int_{\Gamma_c}\left(p_x\frac{\partial u_x^{\mathrm{aux}}}{\partial x} + p_x^{\mathrm{aux}}\frac{\partial u_x}{\partial x} + p_y\frac{\partial u_y^{\mathrm{aux}}}{\partial x} + p_y^{\mathrm{aux}}\frac{\partial u_y}{\partial x}\right)Q\mathrm{d}\Gamma \tag{28}$$

where superscript "aux" denotes auxiliary fields.

The interaction energy integral is related to the SIFs as follows [21]:

$$M^{(1,2)} = \frac{2}{E^*}(K_{\mathrm{I}}^{(1)}K_{\mathrm{I}}^{(2)} + K_{\mathrm{II}}^{(1)}K_{\mathrm{II}}^{(2)}) \tag{29}$$

where E^* is defined in terms of material parameters E (elastic modulus) and ν (Poisson ratio) as

$$E^* = \begin{cases} E, & \text{plane stress} \\ \dfrac{E}{1-\nu^2}, & \text{plane strain} \end{cases} \tag{30}$$

The stress intensity factors for the XFEM state $K_{\mathrm{I}}^{(1)}$ and $K_{\mathrm{II}}^{(1)}$ are given by selecting $K_{\mathrm{I}}^{(2)}=1$ and $K_{\mathrm{II}}^{(2)}=0$, followed by $K_{\mathrm{I}}^{(2)}=0$ and $K_{\mathrm{II}}^{(2)}=1$ such that $K_{\mathrm{I}}^{(1)}$ and $K_{\mathrm{II}}^{(1)}$ are

$$K_{\mathrm{I}}^{(1)}=\frac{E^{*}}{2}I^{(1,\text{mode I})} \tag{31}$$

where $I^{(1,\text{mode I})}$ is the interaction integral for $K_{\mathrm{I}}^{(2)}=0$ and $K_{\mathrm{II}}^{(2)}=0$ and

$$K_{\mathrm{II}}^{(1)}=\frac{E^{*}}{2}I^{(1,\text{mode II})} \tag{32}$$

where $I^{(1,\text{mode I})}$ is the interaction integral for $K_{\mathrm{I}}^{(2)}=0$ and $K_{\mathrm{II}}^{(2)}=1$. Once SIFs are obtained, fracture parameters θ_{c} can be easily computed.

4.2 Crack growth criterion

There are several criteria for predicting crack growth direction in homogeneous materials. The maximum circumferential stress criterion [14] which is a commonly used criterion, is adopted herein. The maximum circumferential stress criterion states that the crack will propagate from its tip when equivalent stress intensity factor $K_{\mathrm{I}}^{\mathrm{eq}}$ is greater than fracture toughness K_{IC}. According to this criterion, the crack growth occurs in a direction perpendicular to the maximum principal stress. Thus, at each crack tip, the angle of crack growth θ_{c} is given by

$$\theta_{\mathrm{c}}=2\arctan\frac{1}{4}\left(K_{\mathrm{I}}\big/K_{\mathrm{II}}\pm\sqrt{\left(K_{\mathrm{I}}/K_{\mathrm{II}}\right)^{2}+8}\right) \tag{33}$$

where K_{I} and K_{II} are the mixed-mode stress intensity factors.

According to this criterion, the equivalent mode-I SIF is obtained as

$$K_{\mathrm{I}}^{\mathrm{eq}}=\frac{1}{2}\cos\left(\frac{\theta_{\mathrm{c}}}{2}\right)[K_{\mathrm{I}}(1+\cos\theta_{\mathrm{c}})-3K_{\mathrm{II}}\sin\theta_{\mathrm{c}}]. \tag{34}$$

5 Coupling solution procedure

The described time-dependent non-linear problem of hydraulic fracture propagation is solved using an iterative solution procedure. Iterative procedure is required to bring the fluid-flow, rock deformation and fracturing processes in equilibrium at every propagation step. The solution process consists of the following operations:

1) The fracture width w is obtained from XFEM analysis under the given initial load and initial crack length. The theoretical apertures w in this model have to be converted to physical apertures w_{eq} using Eq. (25).

2) Solve the water pressure p by Eq. (24). The obtained water pressure distribution p is imposed on the engineering structure to perform XFEM analysis. The water pressure p is solved iteratively using reasonable tolerance on the water pressure difference to judge whether the solution has converged. Once this is satisfied, we go to the next step.

3) Calculate the equivalent stress intensity factor $K_{\mathrm{I}}^{\mathrm{eq}}$; if $K_{\mathrm{I}}^{\mathrm{eq}}$ is less than K_{IC}, go to next step; if $K_{\mathrm{I}}^{\mathrm{eq}}$ is more than K_{IC}, calculate the propagation direction and step length based on the propagation criterion, then go back to step 1.

4) The water pressure at the edge of crack is increased by the time step, go back to step 1.

6 Numerical examples

In order to illustrate the accuracy and versatility of the extended finite element method in modeling of the hydraulic fracturing problem, several numerical examples are presented. The calculation of the stress intensity factors is performed with the domain form of the interaction integral as detailed in the previous section.

6.1 Edge-cracked plate under uniform surface tractions

The first example is chosen to demonstrate the accuracy of stress intensity factor obtained by the proposed XFEM modeling of hydro-mechanical analysis. A square plate with an edge crack under uniform water pressure is shown in Fig. 6. The chosen plate dimensions are a width of 3 m and a height of 3 m with an edge crack of length 1.2 m. The material is linearly elastic with elastic modulus E=10 MPa and the Poisson ratio ν=0.3. The uniform water pressure p=1 Pa is imposed on the crack surface. Square plane stress quadrilateral elements with a structured mesh are used.

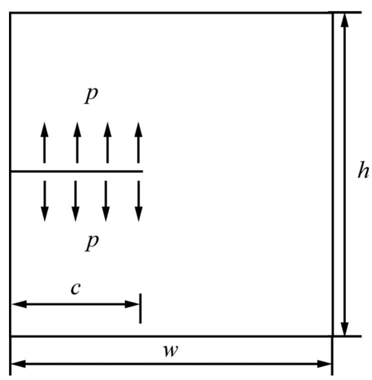

Fig. 6 Edge-cracked plate under water pressure

The stress intensity factor is calculated based on the proposed XFEM modeling of hydro-mechanical analysis considering water pressure along the crack surface. No analytical solutions and numerical results in the literature are compared with the present results. According to superposition principle, the stress intensity factors for edge-cracked plate under uniform surface tractions and edge-cracked plate under tension are approximately equal. The case of a square plate with an edge crack under tension is shown in Fig. 7. All the parameters

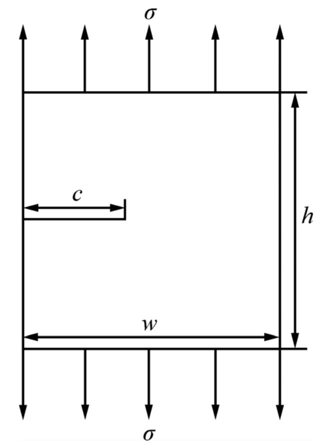

Fig. 7 Edge-cracked plate under tension

including geometry and material properties needed for simulation are considered similar to the previous example. The theoretical Mode I stress intensity factor $K_{\mathrm{I}}^{\mathrm{exac}}$ for this case is given as

$$K_{\mathrm{I}}^{\mathrm{exac}}=\left[1.12-0.231\left(\frac{c}{w}\right)+10.55\left(\frac{c}{w}\right)^2-21.72\left(\frac{c}{w}\right)^3+\right.$$
$$\left.30.39\left(\frac{c}{w}\right)^4\right]\sigma\sqrt{\pi c} \tag{35}$$

where σ is the applied stress. To compare the calculated and theoretical values, the stress intensity factors are normalized:

$$K_{\mathrm{I}}^{\mathrm{N}}=\frac{K_{\mathrm{I}}^{\mathrm{XFEM}}}{K_{\mathrm{I}}^{\mathrm{exac}}} \tag{36}$$

where $K_{\mathrm{I}}^{\mathrm{exac}}$ is given by Eq. (35) and $K_{\mathrm{I}}^{\mathrm{XFEM}}$ is the value calculated by the XFEM analysis using the domain form of the interaction integral. The normalized results for the various mesh density are given in Table 1.

Table 1 Normalized SIF values for various mesh density

Mesh density	$K_{\mathrm{I}}^{\mathrm{N}}$
2025	0.9334
3969	0.9534
5625	0.9758
8649	0.9825
11025	0.9971
15129	0.9996

Figure 8 shows the effect of mesh density on normalized SIF. It can be noticed from Fig. 8 that the good accuracy of computational results can be obtained in the case of coarse mesh and the error decreases with the increase of element number. The mesh density has no more influence on the normalized SIF when the element number is around 6000.

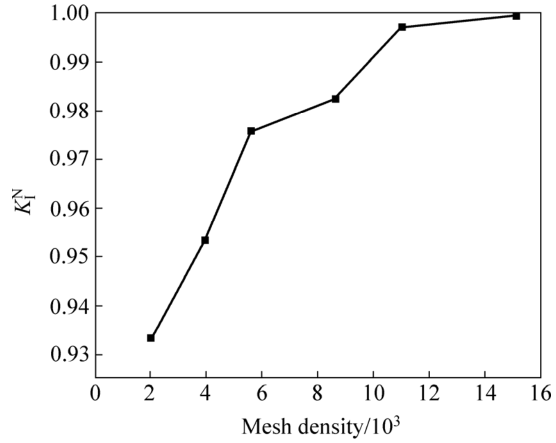

Fig. 8 Effect of mesh density on SIF

Figure 9 shows the SIFs for various crack lengths with 15129 elements in the full domain. It can be noticed from Fig. 9 that the results for the SIFs obtained by XFEM are in excellent agreement with the exact solution for the entire crack length of c/w.

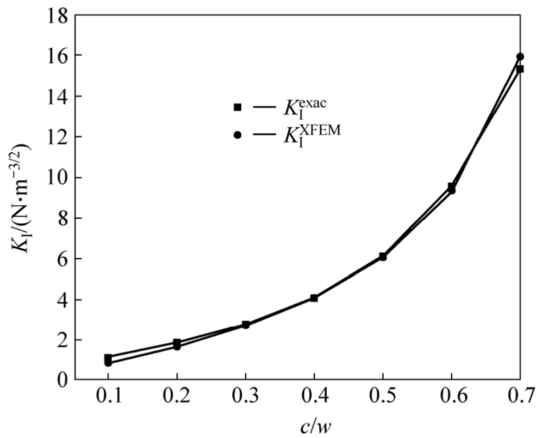

Fig. 9 SIFs for various crack lengths

6.2 XFEM modeling of hydraulic fracturing for rock sample

The second example is chosen to demonstrate the performance of proposed computational algorithm for the hydro-mechanical analysis of an impermeable discontinuity in the rock, as shown in Fig. 10. The

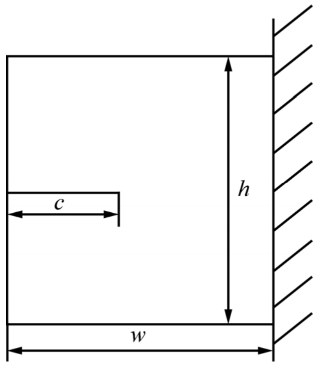

Fig. 10 Geometry model of specimen

chosen sample dimensions are a width of 10 m and a height of 10 m. The edge crack has an initial length of 2 m. The material properties used in the analysis are chosen to be elastic modulus E=39.2 GPa, ν=0.25 and the plane fracture toughness K_{IC}=8.5×10^6 N·m$^{-3/2}$. The sample is constrained at the right boundary and the gravity is ignored while the water pressure p_0=5 MPa is imposed at the edge of crack. We assume the rock joint with a typical JRC value of 10.

In the numerical model, a uniform mesh consisting of 25×25 elements is considered and quasi-static crack growth is governed by the maximum circumferential stress criterion. The change in crack length for each step is taken to be a constant crack growth increment Δc=0.4, and the crack is grown for 5 steps. The specific crack propagations in an impermeable elastic formation at step 2, 5 and deformation are shown in Fig. 11. It can be seen from Fig. 11 that the water pressure loading makes the crack open and propagate along the crack face. Our results are similar to those in Ref. [11]. The corresponding normal and shear stress contours are shown in Fig. 12. It can be seen that the stress concentration near crack tip is very obvious.

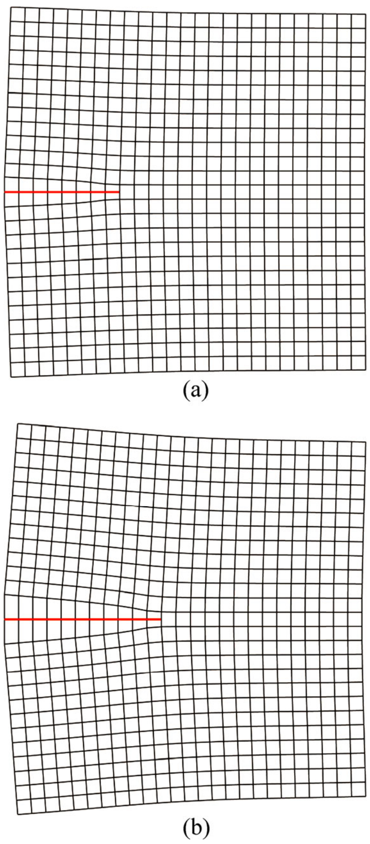

Fig. 11 Deformed shape and crack propagation path: (a) Crack propagation path after 2 steps; (b) Crack propagation path after 5 steps

Table 2 gives the position and SIF of the top crack tip at each step of the simulation. Figure 13 shows the

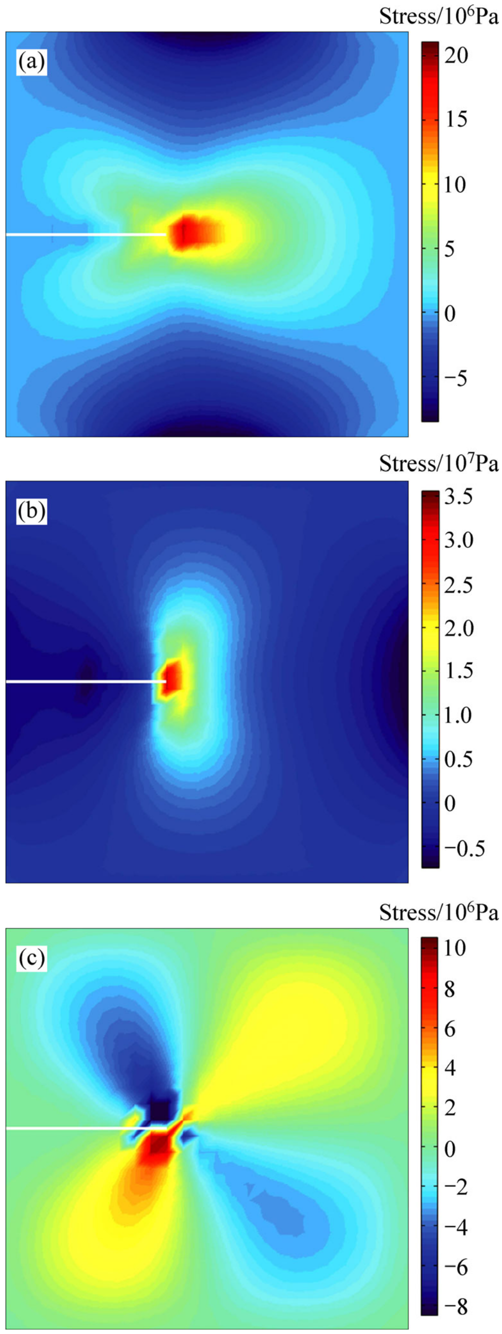

Fig. 12 Normal and shear stress contours: (a) Normal stress σ_{xx}; (b) Normal stress σ_{yy}; (c) Shear stress τ_{xy}

Table 2 Position and SIFs for crack tip

Step	Tip position		K_I/(N·m$^{-3/2}$)
	x/m	y/m	
Initial	2.0	5.0	1.2041×10^7
1	2.4	5.0	1.4417×10^7
2	2.8	5.0	1.7203×10^7
3	3.2	5.0	2.3177×10^7
4	3.6	5.0	2.8018×10^7
5	4.0	5.0	3.2763×10^7

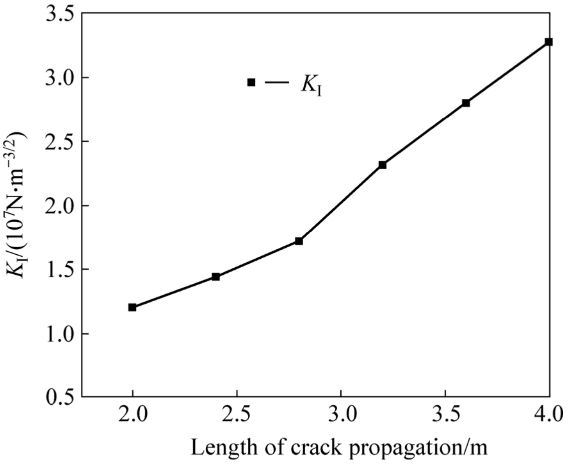

Fig. 13 Relationship between SIF at crack tip and crack propagation length

relationship between the SIF at the crack tip and the crack growth length during the crack propagation. It can be seen from Fig. 13 that the mode ISIF at the crack tip increases with the increase of crack propagation length. The results show that the crack propagation is non-steady under the water pressure loading.

The simulation result for the fracture opening width under different crack propagation step is shown in Fig. 14. It is observed from Fig. 14 that with the propagation of the crack, the crack opening width increases. Figure 15 displays the distribution of water pressure in the direction of the hydraulic fracture propagation after different crack propagation step. It is observed that first water pressure along crack face significantly decreases and then rapidly develops to full head after the hydraulic fracture propagation. The main reason for this result is that with the increase of the crack opening width, the resistance of water flow into the fracture reduces, so the water pressure along crack face is rapidly developed to full head. Simulated results using XFEM are in good agreement with the experimental

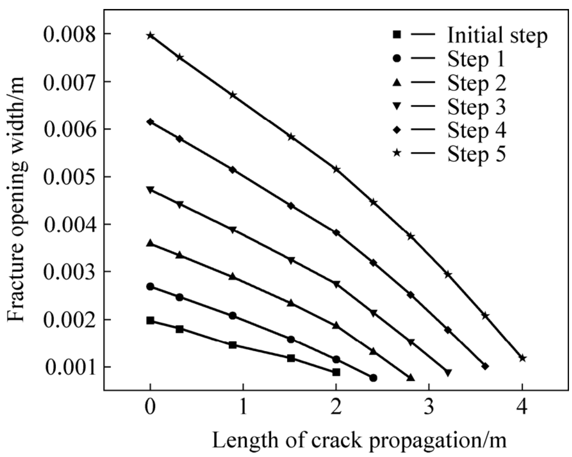

Fig. 14 Fracture opening width under different crack propagation step

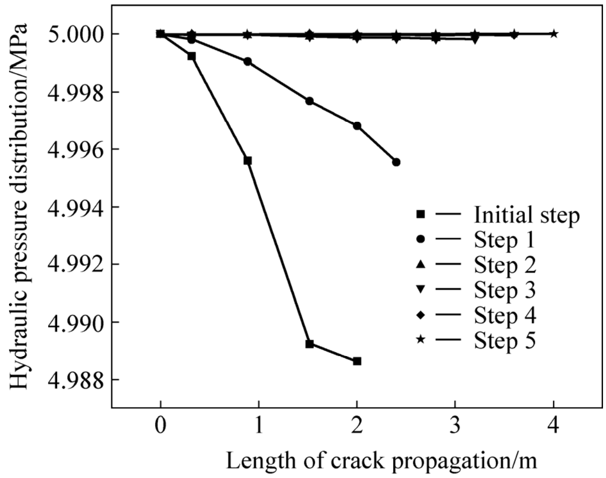

Fig. 15 Hydraulic pressure distribution along crack face under different crack propagation step

results represented by BRÜHWILER and SAOUMA [22]. Excellent agreement between the two solutions demonstrates the capability of the proposed model in simulating hydraulic fracture propagation.

7 Conclusions

A coupled numerical model is developed for the modeling of the hydraulic fracture propagation in rock using the extended finite element method in conjunction with a hydro-mechanical model. The governing equation of XFEM for hydraulic fracture modeling is derived by the virtual work principle of the fracture problem considering the water pressure on crack surface. A hydro-mechanical model of rock with a single fracture initially filled by saturation water is introduced. The coupling relationship between water pressure gradient on crack surface and fracture opening width is obtained by semi-analytical and semi-numerical method. This method simplifies coupling analysis iteration and improves computational precision. Then, numerical examples were analyzed to demonstrate the performance and capability of proposed computational algorithm in modeling of the hydraulic fracturing problem. The first example was selected to deal with the hydro-mechanical analysis of a plate with an edge crack to verify the stress intensity factor obtained from the numerical analysis with available reference results. The second example was chosen to perform the XFEM hydro-mechanical analysis of an impermeable discontinuity in the rock. The results show that the XFEM with remeshing avoided is needed to accurately predict the hydraulic fracture propagation, and the XFEM with remeshing avoided can provide an effective tool for carrying out hydraulic fracture growth in the rock.

References

[1] ADACHI J I, DETOURNAY E. Plane strain propagation of a hydraulic fracture in a permeable rock [J]. Engineering Fracture Mechanics, 2008, 75(16): 4666−4694.

[2] DETOURNAY E. Propagation regimes of fluid-driven fractures in impermeable rocks [J]. International Journal of Geomechanics, 2004, 4: 35−45.

[3] GARAGASH D I. Plane-strain propagation of a fluid-driven fracture during injection and shut-in: Asymptotics of large toughness [J]. Engineering Fracture Mechanics, 2006, 73(4): 456−481.

[4] HU J, GARAGASH D I. Plane-strain propagation of a fluid-driven crack in a permeable rock with fracture toughness [J]. Journal of Engineering Mechanics, 2010, 136(9): 1152−1166.

[5] MITCHELL S L, KUSKE R, PEIRCE A P. An asymptotic framework for the analysis of hydraulic fractures: The impermeable case [J]. Journal of Applied Mechanics, 2006, 74(2): 365−372.

[6] ADACHI J, SIEBRITS E, PEIRCE A, DESROCHES J. Computer simulation of hydraulic fractures [J]. International Journal of Rock Mechanics and Mining, 2007, 44(5): 739−757.

[7] SIMONI L, SECCHI S. Cohesive fracture mechanics for a multi-phase porous medium [J]. Engineering Computations, 2003, 20(5): 675−698.

[8] SECCHI S, SIMONI L, SCHREFLER B A. Mesh adaptation and transfer schemes for discrete fracture propagation in porous materials [J]. International Journal for Numerical and Analytical Methods in Geomechanics, 2007, 31(2): 331−345.

[9] SEGURA J M, CAROL I. Coupled HM analysis using zero-thickness interface elements with double nodes. Part I: Theoretical model [J]. International Journal for Numerical and Analytical Methods in Geomechanics, 2008, 32(18): 2083−2101.

[10] BELYTSCHKO T, BLACK T. Elastic crack growth in finite elements with minimal remeshing [J]. International Journal for Numerical Methods in Engineering, 1999, 45(5): 601−620.

[11] REN Qing-wen, DONG Yu-wen, YU Tian-tang. Numerical modeling of concrete hydraulic fracturing with extended finite element method [J]. Science in China Series E: Technological Sciences, 2009, 52(3): 559−565. (in Chinese)

[12] LECAMPION B. An extended finite element method for hydraulic fracture problems [J]. Communications in Numerical Methods in Engineering, 2009, 25(2): 121−133.

[13] MOHAMADNEJAD T, KHOEI A R. Hydro-mechanical modeling of cohesive crack propagation in multi-phase porous media using the extended-FEM technique [J]. International Journal for Numerical and Analytical Methods in Geomechanics, 2013, 37(10): 1247−1256.

[14] MOËS N, DOLBOW J, BELYTSCHKO T. A finite element method for crack growth without remeshing [J]. International Journal for Numerical Methods in Engineering, 1999, 46 (1): 131−150.

[15] FLEMING M, CHU Y A, MORAN B. Enriched element free Galerkin methods for crack tip fields [J]. International Journal for Numerical Methods in Engineering, 1997, 40(8): 1483−1504.

[16] LI Zong-li, WANG Ya-hong, REN Qing-wen. Numerical simulation model of hydraulic fracturing of rock with a single fracture under natural hydraulic power [J]. Chinese Journal of Rock Mechanics and Engineering, 2007, 26(4): 727−733. (in Chinese)

[17] BARTON N, BANDIS S, BAKHTAR K. Strength, deformation and conductivity coupling of rock joints [J]. International Journal of Rock Mechanics and Mining Sciences & Geomechanics Abstracts, 1985, 22(3): 121−140.

[18] BARTON N, QUADROS E F. Joint aperture and roughness in the prediction of flow and groutability of rock masses [J]. International Journal of Rock Mechanics and Mining Sciences, 1997, 34(3/4): 252.e1−252.e14.

[19] WALTERS M C, PAULINO G H, DODDS R H. Interaction integral procedures for 3-D curved cracks including surface tractions [J]. Engineering Fracture Mechanics, 2005, 72(11): 1635−1663.

[20] FLEMING M, CHU Y A, MORAN B, BELYTSCHKO T. Enriched element free Galerkin methods for crack tip fields [J]. International Journal for Numerical Methods in Engineering, 1997, 40(8): 1483−1504.

[21] WU B, LI Z. Static reanalysis of structures with added degrees of freedom [J]. Communications in Numerical Methods in Engineering, 2006, 22(4): 269−281.

[22] BRÜHWILER E, SAOUMA V E. Water fracture interaction in concrete-part I: Fracture properties [J]. ACI Materials Journal, 1995, 92(3): 296−303.

(Edited by YANG Hua)